Simulations and Parameter Estimation for Extreme-Mass-Ratio Inspirals

Author: Héctor de la Rasilla Díaz, hdelardi8@alumnes.ub.edu
Facultat de Física, Universitat de Barcelona, Diagonal 645, 08028 Barcelona, Spain.

Advisor: Carlos Fernandez Sopuerta, carlos.f.sopuerta@csic.es and Tutor: Oleg Bulashenko, oleg@fqa.ub.edu

Abstract: Extreme mass-ratio inspirals (EMRIs) are considered to be among the most promising sources of low-frequency gravitational waves for the future space-based detector LISA. In this project, the EMRI waveforms are simulated using the analytic kludge approach, which is based on post-Newtonian approximations. The signal-to-noise ratio (SNR) is then computed for various scenarios. To assess the ability to extract physical parameters from the observed signals, a Fisher matrix analysis is performed to estimate the precision of parameters such as mass, spin, eccentricity and luminosity distance. The present study explores how the numerical derivative step size, the compact object mass, and the integration time affect parameter estimation accuracy. Our findings quantify that extending the observation time and considering more massive compact objects lead to substantial enhancements in parameter estimation precision, underscoring their critical importance for future LISA data analysis emphasising the significance of these factors in the analysis of LISA data.
Keywords: General Relativity, Gravitational Waves, Black Holes, Signal-to-Noise Ratio.
SDGs: 4 (Quality Education)

I. INTRODUCTION

Extreme mass-ratio inspirals (EMRIs) are a primary source of gravitational waves (GWs), which LISA, an ESA space mission for a space-based gravitational wave observatory that is already in the implementation phase, will detect [1]. This EMRI system consists of a stellar-mass compact object (CO), typically a black hole or a neutron star, inspiralling into a massive black hole (MBH) located in a galactic centre. The masses of the MBH range from approximately $\sim 10^5$-$10^7 M_\odot$, and for the CO, from $\sim 1-50 M_\odot$. Because of the large mass ratios involved, the system orbits many times before plunging, losing energy and emitting low-frequency gravitational waves (in the mHz regime) [2].

EMRIs serve as ideal astrophysical laboratories due to their strong-field regime, enabling precise tests of General Relativity. The many orbital cycles in LISA's frequency range mean even tiny deviations from Kerr geometry will affect the waveform. In contrast to comparable-mass quasi-circular binaries, which are discernible by ground-based detectors (if they are in the stellar-mass range), EMRI systems are expected to exhibit significant eccentricity and orbital inclination throughout their inspiral phase. This requires the utilisation of waveform models that incorporate multiple harmonics and relativistic corrections over extended timescales. A comparison of the signal measured by LISA with template waveforms is anticipated, with the objective of extracting parameters such as the mass of the MBH or its spin.

These theoretical waveforms are generated using post-Newtonian (PN) approximations of General Relativity. This topic is discussed in more detail in Section II [3].
Furthermore, determining the precision with which we can estimate the values from our waveform model is of particular interest. This objective can be accomplished through the implementation of parameter estimation techniques. Additionally, it is then possible to compare how variation in different parameters affects this estimate.

The main objective of this project is to simulate EMRI waveforms and analyse the precision with which LISA will be able to estimate the physical parameters of these systems. The influence of the compact object mass, the total observation time, and the numerical step size in derivative calculations is given particular attention. In order to address the objectives mentioned above, the paper is structured in three main sections. Firstly, the fundamental equations governing the orbital evolution and generation of waveforms are presented in Section II. Secondly, the numerical implementation and analysis of results is detailed in Section III. Finally, the conclusions obtained are presented in Section IV.

II. THEORETICAL FRAMEWORK OF EMRI WAVEFORMS AND PARAMETER ESTIMATION

A. EMRI Orbital Evolution and Waveform Generation

The PN approximations can be used to calculate the evolution of various parameters. These include the eccentricity (e), the frequency (ν), the mean anomaly (Φ), the angle between $\hat{L} \times \hat{S}$ and pericentre ($\tilde{\gamma}$), and the azimuthal direction of $\hat{L}$. This can be done using the Equations presented in the Appendix (A1).
This determination is followed by the computation of the waveform as outlined below:

$$h_{\alpha,n}(t) = \frac{1}{D}\frac{\sqrt{3}}{2}\left[F_\alpha^+(t)A_n^+(t) + F_\alpha^\times(t)A_n^\times(t)\right], \quad (1)$$

where $F_\alpha^{+,\times}(t)$ represent the antenna pattern functions and the n-harmonic components of the polarisation coefficients, respectively. The former is applicable to the + polarisation, while the latter is applicable to the × polarisation. The total waveform is the sum of all the harmonics:

$$h_\alpha(t) = \sum_n h_{\alpha,n}(t), \tag{2}$$

making $\alpha = I, II$ reference to each of the LISA independent interferometric channels. After obtaining the complete waveform, the next step is the signal analysis.

B. Quantifying Signal Detectability: The Signal-to-Noise Ratio

The data stream produced by LISA consists of both the GW signal and instrumental noise. For each detector channel α the observed signal can be written as:

$$s_\alpha(t) = h_\alpha(t) + n_\alpha(t)\,, \tag{3}$$

where h_α(t) represents the GW waveform and n_α(t) denotes the noise contribution in that channel. Assuming that this form of noise is Gaussian and stationary, the following definition of an inner product is proposed by Cutler and Flanagan [4]:

$$(\mathbf{a}|\mathbf{b}) = 2\sum_\alpha \int_0^\infty \mathrm{d}f \frac{\tilde{a}_\alpha^*(f)\tilde{b}_\alpha(f) + \tilde{a}_\alpha(f)\tilde{b}_\alpha^*(f)}{S_n(f)}\,, \tag{4}$$

where $\tilde{a}(f)$ denotes the Fourier transform of $a(t)$, and $S_n(f)$ is the one-sided power spectral density (PSD) of the noise for all the channels (for simplicity they are assumed to be statistical equivalent). Using this inner product, the signal-to-noise ratio (SNR) for a given waveform $h(t)$ is given by:

$$\mathrm{SNR}^2 \equiv \sqrt{(\mathbf{h}|\mathbf{h})}\,. \tag{5}$$

In practice, this evaluates to:

$$\mathrm{SNR}^2 = 4\sum_\alpha \int_0^\infty \mathrm{d}f \frac{\tilde{h}_\alpha^*(f)\tilde{h}_\alpha(f)}{S_n(f)}\,. \tag{6}$$

C. Precision Measurement: The Fisher Information Matrix Approach

A central objective in gravitational wave data analysis is to determine the accuracy with which physical parameters λ^a of a gravitational wave source can be estimated from the observed signal. Given the assumptions outlined above about the noise, the expected statistical error in estimating a given parameter λ^a can be approximated using the inverse of the Fisher information matrix. Specifically, the minimum standard deviation in parameter λ^a is given (via the Cramer-Rao bound) by:

$$\Delta\lambda^a \geq \sqrt{(\Gamma^{-1})^{aa}}\,, \tag{7}$$

where $(\Gamma^{-1})^{aa}$ denotes the a-th diagonal element of the inverse Fisher matrix. In the high signal-to-noise regime this coincides, with great approximation, with the corresponding component of the covariance matrix. The Fisher matrix itself is defined, in the frequency domain (using the scalar product of Eq. (4)) as:

$$\Gamma_{ab} \equiv \left(\frac{\partial \mathbf{h}}{\partial\lambda^a}\middle|\frac{\partial \mathbf{h}}{\partial\lambda^b}\right)\,, \tag{8}$$

where h is the waveform in Eq. (1). The derivatives $\partial\mathbf{h}/\partial\lambda^a$ are typically computed numerically as it is very difficult to find analytical approximations. In this work, the five-point central difference formula is employed for this computation, which offers a fourth-order accurate approximation:

$$\begin{aligned}\frac{dh}{dx} &= \frac{1}{12\epsilon}[h(x-2\epsilon) - h(x+2\epsilon) + 8h(x+\epsilon) \\ &- 8h(x-\epsilon)] + \mathcal{O}(\epsilon^4)\,.\end{aligned} \tag{9}$$

The choice of the finite difference step size ϵ is critical. If ϵ is too large, the derivative approximation suffers from truncation error; instead, if it is too small, numerical round-off errors may dominate. Thus, careful tuning of ϵ is necessary to ensure accurate and stable estimation of the Fisher matrix elements [5].

Having established a theoretical framework for our simulations and computations, the subsequent step is to implement these equations and procedures numerically. The initial step in this process is to calculate the signal-to-noise ratio (SNR) for typical EMRI configurations. This will enable an assessment of the detectability of these signals.

III. NUMERICAL IMPLEMENTATION AND ANALYSIS OF PARAMETER ESTIMATION

A. Simulating EMRIs and Assessing Detectability (SNR)

To see how this model of waveforms works, let us simulate an EMRI system during 1 year of evolution and calculate its SNR. The EMRI parameters are set as follows: $M = 10^6\mathrm{M}_\odot$, $\mu = 10\mathrm{M}_\odot$, $\mathrm{S/M}^2 = 0.6$, $e_0 = 0.4$, $cos(\lambda) = \sqrt{3}/2$, $\alpha_0 = 0.2$ rad, $\theta_s = 0.1$ rad, $\Phi_k = 1.57$ rad, $\theta_k = 0.3$ rad, $D_L = 1$ Gpc, $\nu_0 = 0.6 \times 10^{-3}$ Hz, $\Phi_0 = 1.57$ rad, $\gamma_0 = 0$ rad.

The evolution waveform is shown in Figure 1 returns a SNR = 11.69, which is a pretty good value and matches what was expected. Once it has been established that the signals are detectable (SNR > 10, the standard threshold for parameter analysis [2]), the next natural step is

to determine what estimation accuracy can be achieved using Fisher matrix analysis. As articulated by Barack and Cutler [3], this methodology is especially well-suited for EMRIs, given their elevated signal-to-noise ratio and extensive duration within the LISA band. The Fisher matrix has been demonstrated to facilitate the quantification of the expected errors through the Cramér-Rao limit [6], provided that SNR > 10, as evidenced by the extant literature.

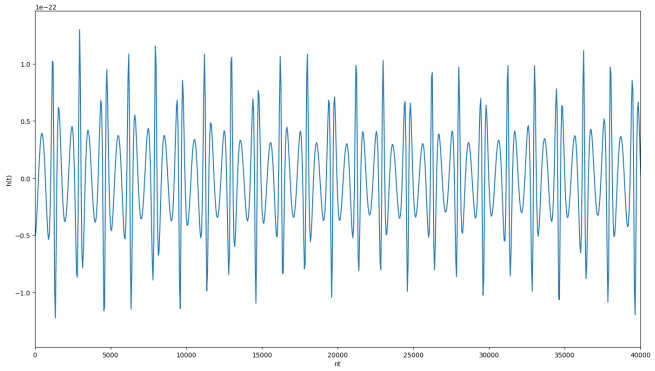

FIG. 1: Waveform of an EMRI system with typical parameters. It shows a section of the gravitational wave signal h(t) integrated during 1 year of evolution for a $10M_\odot$ compact object orbiting a $10^6 M_\odot$ central black hole with initial eccentricity $e_0 = 0.4$. The orbital parameters are: $S/M^2 = 0.6$, $\cos\lambda = \sqrt{3}/2$, D_L=1 Gpc, $\nu_0 = 0.6 \times 10^{-3}$ Hz.

The same simulation for a CO mass $\mu = 1M_\odot$ results in a SNR = 11.63, almost the same as in the previous case, but smaller.

B. Optimizing Numerical Derivatives: Determining the Fisher Matrix Step Size

Performing numerical differentiation implies the problem of choosing the step size ϵ. There are two error sources: firstly, rounding error, which occurs when steps are too short; and secondly, truncation error, which arises from truncating the Taylor expansion of the derivative to order n and it decreases as $\epsilon \to 0$.

One method of determining the correct value for the step is to compute the Fisher matrix element Γ_{aa} using different values for ϵ in the differentiation and subsequently search for the range of values for which the result is stable. As illustrated in Figure 2, the behaviour of the matrix element varies with different steps.

The result indicates the presence of a stable zone with a value of approximately $\epsilon \sim 10^{-4}$ for the step. This value can be considered a satisfactory outcome. It is evident that the rounding error is not apparent, which can be attributed to the fact that the step is not sufficiently small.

The following steps presented in Table I have been identified as offering the greatest stability in the context of

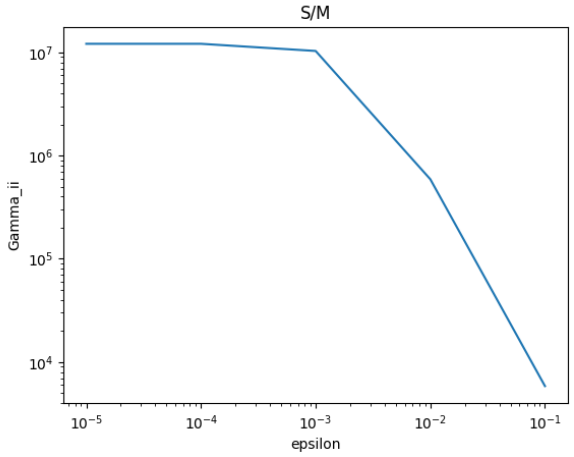

FIG. 2: Step size ϵ stability analysis for the computation of numerical derivatives in the Fisher matrix. It shows the variation of the diagonal component Γ_{aa} of the Fisher matrix as a function of ϵ (logarithmic scale). The stable zone ($\epsilon \sim 10^{-4}$) is identified where Γ_{aa} becomes step-independent. Truncation errors dominate at large ϵ ($> 10^{-3}$), while rounding errors appear for $\epsilon < 10^{-6}$.

the remaining parameters.

To make the parameter estimation analysis more tractable and computationally efficient, the Fisher matrix was computed using a reduced set of parameters, while keeping the rest fixed at their fiducial values. The selected subset includes parameters with strong physical relevance and a significant impact on the waveform: the logarithm of the central black hole mass ln(M), the dimensionless spin S/M^2, the logarithm of the compact object mass $\ln\mu$, the initial eccentricity e_0, and the luminosity distance D_L. This restriction allows us to focus on the most informative parameters while reducing numerical noise and computational cost.

λ^a	ln(M)	S/M^2	ln(μ)	e_0	D_L
ϵ	10^{-4}	10^{-4}	10^{-3}	10^{-4}	10^{-3}

TABLE I: Optimal step sizes (ϵ) for numerical derivatives in the Fisher matrix calculation. Note the variation in orders of magnitude between parameters: while ln(M) and e_0 require $\epsilon \sim 10^{-4}$, parameters such as S/M^2 allow larger step sizes ($\epsilon \sim 10^{-3}$).

It is also worthy to note that the larger the ϵ, the faster the calculation of the Fisher matrix is executed.

Having determined the optimal step size, the next step is to investigate how different physical parameters, initially the mass of the compact object, affect the accuracy of our estimates.

C. Baseline Parameter Estimation: Initial Results and Correlations

Considering the epsilon values in Table I, the Fisher matrix is computed (see Figure 3).

FIG. 3: Visual representation of the Fisher matrix (absolute values) quantifying the correlations between parameters of the EMRI system. The viridis (logarithmic symmetric) colour scale shows the magnitude of the Γ_{aa} elements. The numerical values show the order of magnitude (scientific format). The structure confirms that: (1) e_0 is the best determined parameter, and (2) there are non-trivial correlations between S/M^2 and $\ln(\mu)$ that affect the error estimation. Data obtained for $\mu = 10M_\odot$ and 1 year of observation.

The elevated values of the components that lie outside the diagonal demonstrate a robust correlation between the parameters. It is noteworthy that each parameter exerts a distinct effect on the waveform.

Then, the next step is to obtain the errors $\Delta\lambda^a$ from the covariance matrix, as explained in Equation 7, and the results are presented in Table II.

λ^a	ln(M)	S/M^2	$\ln(\mu)$	e_0	D_L(Gpc)
$\Delta\lambda_a$	$1.8 \cdot 10^{-4}$	$6.6 \cdot 10^{-4}$	$3.2 \cdot 10^{-3}$	$7.9 \cdot 10^{-5}$	$1.2 \cdot 10^{-1}$
Error%	0.001	0.11	0.14	0.02	12

TABLE II: Parameter estimation accuracy for a $10M_\odot$ compact object (1 year of observation). Absolute ($\Delta\lambda^a$) and relative (%) errors obtained from the diagonal of the Fisher matrix are shown (Eq. 7).

It can be observed that the most accurate parameter is the initial eccentricity e_0, in accordance to its elevated Fisher matrix diagonal value exposed before, and the least accurate is the luminosity distance D_L.

The election of the step size for the derivatives plays a decisive role in Fisher matrix.

ϵ	λ^a	ln(M)	S/M^2	$\ln(\mu)$	e_0	D_L(Gpc)
10^{-2}	$\Delta\lambda_a$	$1.8 \cdot 10^{-2}$	$6.6 \cdot 10^{-4}$	$3.2 \cdot 10^{-3}$	$7.9 \cdot 10^{-5}$	0.12
	Error%	0.13	0.11	0.14	0.02	12
10^{-3}	$\Delta\lambda_a$	$1.8 \cdot 10^{-3}$	$6.6 \cdot 10^{-4}$	$3.2 \cdot 10^{-3}$	$7.9 \cdot 10^{-5}$	0.12
	Error%	0.01	0.11	0.14	0.02	12
10^{-4}	$\Delta\lambda_a$	$1.8 \cdot 10^{-4}$	$6.6 \cdot 10^{-4}$	$3.2 \cdot 10^{-3}$	$7.9 \cdot 10^{-5}$	0.12
	Error%	0.001	0.11	0.14	0.02	12

TABLE III: Parameter accuracy estimates and its relative error for 1 year of evolution for different values for the step size of the M derivative.

The changes in ϵ only affects significantly to the parameter itself, as seen in Table III for the mass of the central black hole. As ϵ value drops, it parameter accuracy estimate decreases proportionally. All the values for the step size are those located in the stable zone discussed previously. Instead, varying the step size of the rest of parameters within the stable range, the parameter accuracy estimates remain constant. It is also more time consuming computing the Fisher matrix with smaller step sizes.

D. Impact of Compact Object Mass on Parameter Precision

The computation is repeated changing the CO mass from $10M_\odot$ to $1M_\odot$ and the following results presented in Table IV are obtained.

λ^a	ln(M)	S/M^2	$\ln(\mu)$	e_0	D_L(Gpc)
$\Delta\lambda_a$	$1.8 \cdot 10^{-3}$	$9.6 \cdot 10^{-3}$	$3.0 \cdot 10^{-1}$	$9.2 \cdot 10^{-4}$	1.3
Error%	0.01	1.6	134	0.23	130

TABLE IV: Parameter accuracy estimates and its relative error with respect the inserted value. All parameters are fixed as previously with CO mass $\mu = 1M_\odot$.

It is observed that the values with the CO mass $10\,M_\odot$ presented in Table II are mostly an order of magnitude smaller than those with CO of $1M_\odot$ presented in Table IV. This shows that higher CO mass implies better accuracy in parameter estimation.
This trend is due to the stronger gravitational wave signal produced by a more massive compact object, resulting in a higher signal-to-noise ratio, as were already prove in Section IIIa. A higher SNR improves the precision with which waveform parameters can be extracted. Furthermore, the bigger the mass ratio, the more the waveform changes, and this reduces the error associated with the main parameters.

E. Influence of Observation Time on Parameter Estimation Accuracy

The next step is to study the effect of the variation of the total integration time on the accuracy of parameter estimation. The previous results were obtained over a period of one year. The same computation was performed for two years and the results are presented in Table V.

λ^a	ln(M)	S/M^2	$\ln(\mu)$	e_0	D_L(Gpc)
$\Delta\lambda_a$	$9.1 \cdot 10^{-5}$	$8.6 \cdot 10^{-5}$	$7.4 \cdot 10^{-4}$	$2.7 \cdot 10^{-5}$	$6.2 \cdot 10^{-2}$
Error%	0.0007	0.01	0.03	0.007	6.2

TABLE V: Parameter accuracy estimates and its relative error with respect the inserted value for 2 years of evolution. All is computed using the step sizes presented in Table I.

A comparison of these results with those obtained after one year of integration reveals a significant decrease in parameter estimation errors, with some values improving by nearly an order of magnitude. This enhancement is anticipated, as an extended observation period enables the detector to accumulate a greater number of signal cycles, thereby enhancing the signal-to-noise ratio (SNR). Furthermore, an extended integration time facilitates the detection of features that evolve more slowly, consequently improving the estimation of parameters such as eccentricity and distance. This shows Fisher matrix accuracy depends strongly on integration time.

IV. CONCLUSIONS AND OUTLOOK

The present project has involved the modelling of extreme mass-ratio inspirals (EMRI) systems and the investigation of the precision with which their physical parameters can be extracted from gravitational-wave signals using the Fisher information matrix formalism.
A crucial step in this study was the generation of theoretical waveforms, based on post-Newtonian approximations of the orbital evolution. The system of coupled ordinary differential equations (ODEs) governing quantities such as the orbital frequency, eccentricity, and precession angles was solved numerically. These evolving parameters were then used to construct the waveform as a sum over harmonics, incorporating the detector's antenna pattern functions. Finally, Fourier transforms of the waveform were computed to obtain the signal in the frequency domain, which is essential for both signal-to-noise ratio (SNR) calculation and Fisher matrix estimation.

The results presented in the preceding section permit the formulation of several conclusions pertinent to the detection and characterisation of EMRI systems with LISA. The SNR obtained for typical EMRI configurations confirms that these signals will be detectable by LISA, even for relatively small compact object masses and moderate eccentricities. The estimation of parameters such as the central massive black hole mass, its spin, and the orbital eccentricity is a viable prospect under realistic conditions. The initial eccentricity was found to be the most precisely determined parameter, while the luminosity distance was found to be the least constrained.

The choice of step size employed in numerical derivatives for the Fisher matrix exerts a substantial influence on the estimated uncertainties. A stable range of step values was identified, which have been shown to provide reliable results. An enhancement in the accuracy of parameters was observed, which increased in proportion to the mass of the compact object and the duration of the integration period. Specifically, the prolongation of the observation period from one to two years led to a reduction in uncertainties by up to an order of magnitude, thereby underscoring the significance of extended duration observations. The analysis demonstrates the effectiveness of the Fisher matrix as a preliminary step towards understanding the parameter estimation capabilities of LISA for EMRI signals.

Acknowledgments

I would like to express my deepest gratitude to my advisor, Carlos F. Sopuerta, for his expert guidance, support, and patience throughout the development of this project. I would also like to thank my tutor, Oleg Bulashenko, for his constructive feedback and support. I am extremely grateful to my family for their unwavering support during my studies. In addition, I would like to express my gratitude to my colleagues for their encouragement, humour, and companionship during challenging times. Finally, I would like to extend my gratitude to my partner, whose unwavering support, patience and love have been essential elements throughout my journey.

[1] N. Afshordi et al. (LISA Consortium Waveform Working Group), Tech. Rep. (2023), 2311.01300.
[2] S. Babak et al., Phys. Rev. D **95**, 103012 (2017), 1703.09722, URL http://dx.doi.org/10.1103/PhysRevD.95.103012.
[3] L. Barack and C. Cutler, Physical Review D **69** (2004), ISSN 1550-2368, URL http://dx.doi.org/10.1103/PhysRevD.69.082005.
[4] C. Cutler and E. Flanagan, Physical Review D **49** (1994), ISSN 0556-2821.
[5] T. Sauer, *Numerical Analysis* (Pearson, 2012).
[6] C. Cutler and M. Vallisneri, Physical Review D **76** (2007), ISSN 1550-2368, URL http://dx.doi.org/10.1103/PhysRevD.76.104018.

Simulacions i estimació de paràmetres per inspirals de raó de massa extrema

Author: Héctor de la Rasilla Díaz, hdelardi8@alumnes.ub.edu
Facultat de Física, Universitat de Barcelona, Diagonal 645, 08028 Barcelona, Spain.

Advisor: Carlos Fernandez Sopuerta, carlos.f.sopuerta@csic.es and Tutor: Oleg Bulashenko, oleg@fqa.ub.edu

Resum: Aquest treball se centra en la simulació de sistemes de raó de massa extrema (EMRI), fonts rellevants d'ones gravitacionals per al futur observatori espacial LISA. Utilitzant aproximacions post-Newtonianes, es calcula l'evolució orbital i la forma d'ona resultant, així com la seva relació amb el senyal que LISA podria detectar. A més, s'aplica el formalisme de la matriu de Fisher per estimar amb quina precisió es poden determinar paràmetres físics com la massa i l'espín del forat negre central, l'excentricitat inicial i la distància de lluminositat. Els resultats mostren que tant la massa de l'objecte compacte com el temps d'integració són factors clau per a millorar la precisió de l'estimació. Aquest estudi contribueix a entendre millor la capacitat de LISA per fer ciència de precisió amb fonts EMRI. **Paraules clau:** Relativitat general, ones gravitacionals, forats negres, raó de senyal i soroll.
ODSs: Aquest TFG està relacionat amb els Objectius de Desenvolupament Sostenible (SDGs)

Objectius de Desenvolupament Sostenible (ODSs o SDGs)

1. Fi de la es desigualtats		10. Reducció de les desigualtats	
2. Fam zero		11. Ciutats i comunitats sostenibles	
3. Salut i benestar		12. Consum i producció responsables	
4. Educació de qualitat	X	13. Acció climàtica	
5. Igualtat de gènere		14. Vida submarina	
6. Aigua neta i sanejament		15. Vida terrestre	
7. Energia neta i sostenible		16. Pau, justícia i institucions sòlides	
8. Treball digne i creixement econòmic		17. Aliança pels objectius	
9. Indústria, innovació, infraestructures			

El contingut d'aquest TFG, com a part d'un grau universitari en Física, s'alinea amb l'ODS 4, especialment amb la fita 4.4, ja que contribueix a l'adquisició de competències científiques i tècniques en l'àmbit de la relativitat i l'anàlisi de dades.

Appendix A: ORBIT EVOLUTION EQUATIONS

In this Appendix are presented the system of coupled ordinary differential equations that governs the orbit evolution of EMRIs:

$$
\begin{aligned}
\frac{de}{dt} =& -\frac{e}{15}(\mu/M^2)(1-e^2)^{-7/2}(2\pi M\nu)^{8/3}\times \\
& \left[(304+121e^2)(1-e^2)(1+12(2\pi M\nu)^{2/3}) - \frac{1}{56}(2\pi M\nu)^{2/3}((8(16705)+(12)(9082)e^2-25211e^4)\right] \\
& + e(\mu/M^2)(S/M^2)cos\lambda(2\pi M\nu)^{11/3}(1-e^2)^{-4}[(1364/5)+(5032/15)e^2+(263/10)e^4], \\
\\
\frac{d\nu}{dt} =& \frac{96}{10\pi}(\mu/M^3)(2\pi M\nu)^{11/3}(1-e^2)^{-9/2}\{[1+(73/24)e^2+(37/96)e^4](1-e^2) \\
& + (2\pi M\nu)^{2/3}[(1273/336)-(2561/224)e^2-(3885/128)e^4-(13147/5376)e^6] \\
& - (2\pi M\nu)(S/M^2)cos\lambda(1-e^2)^{-1/2}[(73/12)+(1211/24)e^2+(3143/96)e^4+(65/64)e^6]\}, \\
\\
\frac{d\Phi}{dt} =& 2\pi\nu, \\
\\
\frac{d\tilde{\gamma}}{dt} =& 6\pi\nu(2\pi M\nu)^{2/3}(1-e^2)^{-1}\left[1+\frac{1}{4}(2\pi M\nu)^{2/3}(1-e^2)^{-1}(26-15e^2)\right] \\
& - 12\pi\nu cos\lambda(S/M^2)(2\pi M\nu)(1-e^2)^{-3/2}, \\
\\
\frac{d\alpha}{dt} =& 4\pi\nu(S/M^2)cos\lambda(2\pi M\nu)(1-e^2)^{-3/2}.
\end{aligned}
\tag{A1}
$$